Am J Physiol Renal Physiol 319: F988–F999, 2020.
First published October 26, 2020; doi:10.1152/ajprenal.00295.2020.

RESEARCH ARTICLE

Beyond the tubule: pathological variants of *LRP2*, encoding the megalin receptor, result in glomerular loss and early progressive chronic kidney disease

Jennifer R. Charlton,[1]* Weizhen Tan,[2]* Ghaleb Daouk,[2] Lisa Teot,[3] Seymour Rosen,[3,4] Kevin M. Bennett,[5] Aleksandra Cwiek,[1] Sejin Nam,[6] Francesco Emma,[7] François Jouret,[8] João Paulo Oliveira,[9] Lisbeth Tranebjærg,[10,11] Carina Frykholm,[12] Shrikant Mane,[13] Friedhelm Hildebrandt,[14] Tarak Srivastava,[15] Tina Storm,[16] Erik Ilsø Christensen,[16] and Rikke Nielsen[16]

[1]*Division of Nephrology, Department of Pediatrics, University of Virginia, Charlottesville, Virginia;* [2]*Division of Nephrology, Massachusetts General Hospital for Children, Boston, Massachusetts;* [3]*Department of Pathology, Boston Children's Hospital, Boston, Massachusetts;* [4]*Department of Pathology, Beth Israel Deaconess Medical Center, Boston, Massachusetts;* [5]*Department of Radiology, Washington University in Saint Louis, St. Louis, Missouri;* [6]*Department of Physics, University of Hawai'i at Manoa, Manoa, Hawai'i;* [7]*Division of Nephrology, Department of Pediatric Subspecialties, Bambino Gesu[a] Children's Hospital-Istituto di Ricovero e Cura a Carattere Scientifico, Rome, Italy;* [8]*Groupe Interdisciplinaire de Génoprotéomique Appliquée, Unit of Cardiovascular Sciences, University of Liège, Liège, Belgium;* [9]*Service of Medical Genetics, São João University Hospital Centre and Faculty of Medicine, University of Porto and i3S-Institute for Health Research and Innovation, Porto, Portugal;* [10]*Department of Clinical Genetics, Rigshospitalet/The Kennedy Centre, Copenhagen, Denmark;* [11]*Institute of Clinical Medicine, University of Copenhagen, The Panum Institute, Copenhagen, Denmark;* [12]*Department of Immunology, Genetics and Pathology, Uppsala University, Uppsala, Sweden;* [13]*Department of Genetics, Yale University School of Medicine, New Haven, Connecticut;* [14]*Department of Medicine, Boston Children's Hospital, Harvard Medical School, Boston, Massachusetts;* [15]*Children's Mercy Hospital, Kansas City, Missouri; and* [16]*Department of Biomedicine, Aarhus University, Aarhus, Denmark*

Submitted 15 June 2020; accepted in final form 19 October 2020

Charlton JR, Tan W, Daouk G, Teot L, Rosen S, Bennett KM, Cwiek A, Nam S, Emma F, Jouret F, Oliveira JP, Tranebjærg L, Frykholm C, Mane S, Hildebrandt F, Srivastava T, Storm T, Christensen EI, Nielsen R. Beyond the tubule: pathological variants of *LRP2*, encoding the megalin receptor, result in glomerular loss and early progressive chronic kidney disease. *Am J Physiol Renal Physiol* 319: F988–F999, 2020. First published October 26, 2020; doi:10.1152/ajprenal.00295.2020.—Pathogenic variants in the *LRP2* gene, encoding the multiligand receptor megalin, cause a rare autosomal recessive syndrome: Donnai-Barrow/Facio-Oculo-Acoustico-Renal (DB/FOAR) syndrome. Because of the rarity of the syndrome, the long-term consequences of the tubulopathy on human renal health have been difficult to ascertain, and the human clinical condition has hitherto been characterized as a benign tubular condition with asymptomatic low-molecular-weight proteinuria. We investigated renal function and morphology in a murine model of DB/FOAR syndrome and in patients with DB/FOAR. We analyzed glomerular filtration rate in mice by FITC-inulin clearance and clinically characterized six families, including nine patients with DB/FOAR and nine family members. Urine samples from patients were analyzed by Western blot analysis and biopsy materials were analyzed by histology. In the mouse model, we used histological methods to assess nephrogenesis and postnatal renal structure and contrast-enhanced magnetic resonance imaging to assess glomerular number. In megalin-deficient mice, we found a lower glomerular filtration rate and an increase in the abundance of injury markers, such as kidney injury molecule-1 and *N*-acetyl-β-D-glucosaminidase. Renal injury was validated in patients, who presented with increased urinary kidney injury molecule-1, classical markers of chronic kidney disease, and glomerular proteinuria early in life. Megalin-deficient mice had normal nephrogenesis, but they had 19% fewer nephrons in early adulthood and an increased fraction of nephrons with disconnected glomerulotubular junction. In conclusion, megalin dysfunction, as present in DB/FOAR syndrome, confers an increased risk of progression into chronic kidney disease.

cationic ferritin-enhanced magnetic resonance imaging; glomerular number; kidney disease etiology; megalin; nephron loss; proximal tubule

INTRODUCTION

Autosomal recessive Donnai-Barrow/Facio-Oculo-Acoustico-Renal (DB/FOAR) syndrome is caused by pathogenic variants in the *LRP2* gene, encoding the receptor megalin (20). Megalin is a 600-kDa endocytic receptor that is present in low amounts in podocytes and abundant at the apical membrane of the renal proximal tubule. It is also located in many extrarenal epithelia, such as the eye, choroid plexus, ear, and embryonic tissues, including the neuroectoderm (11, 13, 14, 22, 31, 33, 39, 40, 42, 48, 49). Consequently, patients with pathogenic variants in *LRP2* exhibit a multifaceted phenotype, including hypertelorism, anomalies of corpus callosum, and high myopia (20). However, reports of patients with only a few of the classical DB/FOAR symptoms and pathogenic variants in *LRP2* have been published (2, 34, 44), suggesting a broader phenotype and potentially a higher prevalence of the disease.

The well-described, clinical renal phenotype of DB/FOAR patients is a tubular defect resulting in low-molecular-weight proteinuria (20, 41), consistent with the known role of megalin as a multiligand receptor. Megalin, in concert with the receptor cubilin, reabsorbs virtually all filtered proteins by endocytosis in the proximal tubule (12). Patients with *LRP2* pathogenic

* J. R. Charlton and W. Tan contributed equally to this work.
Correspondence: R. Nielsen (rn@biomed.au.dk).

variants experience urinary loss of vitamin D-binding protein, retinol-binding protein (RBP), and albumin (1, 27, 41, 46, 47), similar to mouse models with megalin deletion in the kidney (27, 46). Interestingly, urinary loss of low-molecular-weight proteins is reported in DB/FOAR patients no matter the severity of the disease, and a glomerular phenotype has been observed in a few patients (24, 35, 38). Our aim was to establish whether the renal phenotype of this classical tubular disease increases the risk of a glomerular dysfunction and renal decline.

In this study, we show kidney injury and a decline in renal function in a mouse model with embryonic kidney-specific deletion of megalin, mimicking the human phenotype of DB/FOAR syndrome. We provide evidence that DB/FOAR patients develop glomerular proteinuria and chronic kidney disease (CKD) early in life. In the mouse model, we observed that the duration of nephrogenesis was unaffected, but that megalin deficiency resulted in nephron loss and abnormalities in the glomerulotubular junction in early adulthood. Our data suggest that megalin is not only an important tubular receptor, but that it is also required for glomerular health.

METHODS

Patients and families. Nine patients (3 mo to 35 yr of age) from six families were included in the study, and family members were included if available (Supplemental Material, available online at https://doi.org/10.6084/m9.figshare.12993152.v1, includes a description of each family). Each patient was identified by a two-number label, e.g., *patient 1-1*, where the first number stands for the family and the second number stands for the individual. Family members were also designated "carriers" and presented with the family number and a letter (e.g., *carrier 2a*). Each individual was coupled to a symbol, making it possible to see the location of their pathogenic variant in the protein and their urinary protein excretion (see Fig. 2).

Urinary protein excretion. Spot urine samples collected from the patients were combined with a protease inhibitor cocktail (Complete, Roche, Hvidovre, Denmark) and stored at −80°C. Urinary protein excretion was compared with urinary protein excretion in five to nine age-matched healthy individuals. A urinary volume corresponding to 4 μg of creatinine (corresponding to 35 nmol) was analyzed using SDS-PAGE and transferred to an Immobilon FL PVDF transfer membrane (Millipore, Copenhagen, Denmark) using the iBlot Dry Blotting System (Invitrogen, Taastrup, Denmark). Membranes were subsequently blocked and incubated with primary- and fluorophore-coupled secondary antibodies, according to the manufacturer (LI-COR Biosciences, Cambridge, UK). Proteins were detected using the Odyssey infrared imager (LI-COR Biosciences). Urinary albumin, creatinine, and protein were additionally measured in certified biochemical laboratories in the specific countries.

Immunohistochemistry. Renal tissue samples collected from patients for diagnostic purposes were fixed and embedded in paraffin for routine pathology. For light microscope immunohistochemistry, sections from the patients and controls were prepared as previously described (45). Sections were incubated with a primary antibody in 0.01 M PBS, 0.1% BSA, and 0.02 M NaN_3 followed by incubation with horseradish peroxidase-conjugated secondary antibody. Peroxidase labeling was visualized by incubation with diaminobenzidine and 0.03% H_2O_2 for 10 min. Sections were counterstained with Mayer's hematoxylin stain and examined in a Leica DMR microscope equipped with a Leica DFC320 camera. Images were transferred by a Leica TFC Twain 6.1.0 program and processed using Adobe Photoshop 8.0. Fluorescence microscopy was performed by standard methods.

Antibodies. Primary antibodies were as follows: rabbit anti-vitamin D-binding protein (A0021), rabbit anti-transferrin (A0061), rabbit anti-albumin (A0001), rabbit anti-RBP (A0040), rabbit anti-β_2-microglobulin (A0072), and rabbit anti-human IgG (A423) (all polyclonal anti-human antibodies, Dako, Glostrup, Denmark); goat anti- kidney injury molecule (KIM)-1 (R&D) and goat anti-mouse cystatin C (R&D); biotinylated *Lotus tetragonolobus* (*Lotus*) lectin (B-1325, Vector Laboratories); rabbit anti-horse spleen ferritin antibody (F6136; Sigma-Aldrich); mouse anti-synaptopodin antibody (sc-21537; Santa Cruz Biotechnology); rabbit anti-rat cubilin (26); rabbit anti-human megalin (31) (kindly provided by Dr. S. K. Moestrup); and sheep anti-rat megalin (kindly provided by Dr. P. Verroust). Secondary antibodies were as follows: IRDye (LI-COR), Alexa Fluor (Invitrogen), and horseradish peroxidase conjugated (Dako).

Animals. Animal experiments and breeding were approved by the Danish Animal Experiments Inspectorate and performed in the animal facility of Department of Biomedicine, Aarhus University, Aarhus, Denmark. The study adhered to the National Institutes of Health *Guide for the Care and Use of Laboratory Animals*. Female mice with homozygous conditional inactivation of the *Lrp2* gene in the kidney were generated by breeding Tg(Wnt4-Cre)129SvE-F Tac IK or Tg(Wnt4-Cre)C57BL/6JTac transgenic mice with mice bearing a loxP-flanked *Lrp2* allele ($Lrp2^{tm1Tew}$) to create embryonic kidney-specific megalin knockout (KO) mice both on a pure C57BL/6JTac background and a pure 129SvE-F Tac IK background. Embryonic Wnt4 expression occurs in tubular cells and podocytes (36, 46). An outline of the number of animals and strain used in each experiment is shown in Supplemental Table S1. *Cre*-negative littermates served as controls in all experiments. The KO degree was determined by quantitative RT-PCR, but when both kidneys were used for other analyses, the KO degree was determined by immunohistochemical analyses. In general, we observed 80–95% deletion of megalin, but five animals included in the structural analyses had KO degrees in the range of 40–80%.

Mouse kidney function analyses. Glomerular filtration rate (GFR) was investigated by the method of Rieg (32) using intravenous injections of FITC-inulin per gram body weight and measurement of plasma clearance of 60- to 98-day-old mice. The weight of the mice did not differ significantly. Plasma and urine creatinine were determined according to standard procedures (Siemens Diagnostics Clinical Methods for ADVIA 1800) (Jaffe, 74016). Analyses were performed using an autoanalyzer, ADVIA 1800 Chemistry System (Siemens Medical Solutions, Tarrytown, NY). The relative abundance of KIM-1 in urine was measured by Western blot analysis, normalized according to creatinine. *N*-acetyl-β-D-glucosaminidase (NAGase) activity in urine was detected by the end-point fluorometric method, according to Larsen et al. (25).

Cationic ferritin-enhanced magnetic resonance imaging. To label the glomeruli for magnetic resonance imaging (MRI) detection, mice received 5.75 mg/100 g body wt of horse spleen cationic ferritin (CF; F7879, Sigma-Aldrich) at the age of 50–70 days (4, 8). CF was administered in two equal retroorbital injections separated by 90 min under isoflurane anesthesia (4). All animals were euthanized 90 min after the last injection of CF followed by retroaortic perfusion of HBSS followed by perfusion with 2% paraformaldehyde in 0.1 M cacodylate buffer (pH 7.4). One kidney was stored whole in 2% glutaraldehyde/0.1 mol/L cacodylate solution for CFE-MRI, while the other was postfixed with formalin for paraffin embedment. The intact kidney was placed in a customized holder with the capacity to image eight kidneys using a Bruker quadrature RF probe (inner diameter:30 mm). Imaging was performed on a Bruker 7T/30 MRI (Bruker, Billerica, MA) with Siemens software for acquisition and reconstruction (Siemens, Munich, Germany) at the University of Virginia (sequence parameters: 3D T2*-weighted, scan: echo time/repetition time: 20/80 ms; slice thickness: 60 μm, 640 × 640). CF-labeled glomeruli appear as dark spots in the cortex of gradient-echo MR images. This appearance is consistent with previous publications in mouse (4), rat (7), rabbit (9) and ex vivo human (6) MRI, where CF accumulates in the glomerular basement membrane (Supplemental Fig. S1).

Image processing for the number and volume of glomeruli. As in a previous publication (4), the images were manually segmented to separate each kidney from the remaining eight and to remove the medullary region. This allows for the measurement of cortical and medullary volumes. The resolution was increased by linear interpolation to 19.53 × 19.53 × 20 mm using Amira (FEI, Bordeaux, France) software. Three-dimensional (3D) raw data of the segmented kidney were processed in MATLAB (The MathWorks, Natick, MA) to create two sets of two dimensional images along the *x*- and *y*-axes. MIPAR was used to manually adjust contrast (low level, high level, and γ values of 2, 128, and 1.5, respectively). Kidney images were processed using an adaptive thresholding in MIPAR with a threshold of 50% and a window size of 15 pixels. Segmented glomeruli smaller than four voxels were rejected. The glomerular images and segmented medulla regions were analyzed with custom MATLAB scripts to obtain the number of glomeruli (N_{glom}) and apparent volume of glomeruli (aV_{glom}), as previously described (4).

Validation of CF labeling. Immunofluorescence was performed on formalin-fixed kidney tissue from the contralateral kidney that underwent MRI to confirm targeted CF labeling in the glomeruli (Supplemental Fig. S1). Kidney samples were embedded in paraffin, sectioned at four micrometers thick, and rehydrated using Histoclear (National Diagnostics, Atlanta, GA) and graded ethanol dilutions. Antigen retrieval was accomplished by boiling the slides in 10 mM citrate buffer. The tissue was blocked using normal donkey serum (1:10) in 5% of BSA in PBS for 1 h in a humidity chamber. Sections were incubated with the following primary antibodies overnight: *1*) rabbit anti-horse spleen ferritin antibody (concentration: 1:100, F6136; Sigma-Aldrich) and *2*) mouse anti-synaptopodin antibody to highlight podocytes (concentration: 1:200). Secondary antibodies were applied for 2 h at room temperature: donkey anti-rabbit Alexa Fluor 594 (1:200, Life Technologies) and donkey anti-mouse Alexa Fluor 488 (1:250, Life Technologies). To stain nuclei, 4',6-diamidino-2-phenylindole (DAPI) was applied, and each slide was rehydrated. Images were obtained using Microscope Leica Microsystems CMS.

Histological assessment. Kidney samples from the 50- to 70-day group were prepared by standard techniques, embedded in paraffin, and sectioned. The presence of *Lotus* lectin (Vector Laboratories) was identified by treating sections with proteinase K enzymatic digestion followed by biotinylated *Lotus* lectin (1:50 dilution), and the ABC-DAB reaction was induced. Quantitation of proximal tubules was accomplished by analyzing the DAB reaction within each image (ImagePro Plus 5.1, Media Cybernetics, Silver Spring, MD). Renal cortical volume fraction of proximal tubules was measured using a stereologic approach, as described in a previous publication (18). Ten fields were photographed at ×20 magnification in the subcapsular region, and the DAB reaction product was expressed as te percent area value [volume fraction (V_v)]. As *Lotus* lectin staining is specific to mature proximal tubular cells and the papillary collecting duct, the identification of the *Lotus*-positive area is useful for quantifying the preservation of the renal cortex, and the lack of staining present in Bowman's capsule represents disruption of the glomerulotubular connection ("atubular glomeruli"). In essence, the latter fraction includes both

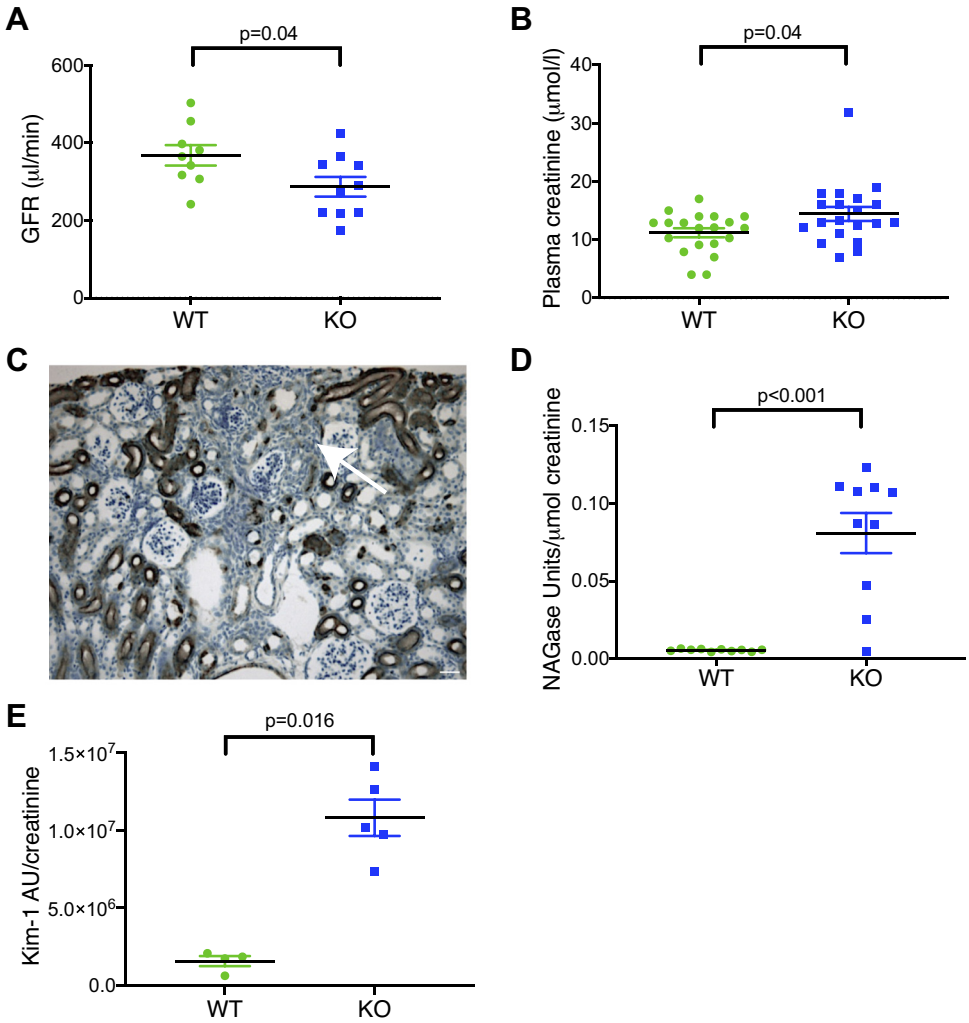

Fig. 1. Renal function in megalin knockout (KO) and wild-type (WT) mice at 60−98 days. *A*: glomerular filtration rate (GFR) measured by FITC-inulin clearance. *B*: plasma creatinine. *C*: representative micrograph showing a megalin KO mouse section stained with *Lotus tetragonolobus* lectin, illustrating normal proximal tubules, sometimes interspaced by areas lacking proximal tubules (arrow). Scale bars = 50 µm. *D*: urinary *N*-acetyl-β-D-glucosaminidase (NAGase) excretion. *E*: urinary kidney injury molecule (KIM)-1 excretion. The number of data points equals *n*. AU, arbitrary units.

real atubular glomeruli and glomeruli assessed at a plane where the junction is not visible. Comparison of *Lotus* lectin-negative glomeruli in the two groups indicates whether there is an increase in real atubular glomeruli in either group. This method has been extensively validated in serial sections (18).

Neonatal cohort. It is not feasible to do CFE-MRI on neonatal mouse kidneys; therefore, the kidneys were prepared and stained with periodic acid-Schiff to identify glomeruli. Mature glomeruli were counted in a midsagittal section at the completion of nephrogenesis, *postnatal day 4*. Using Amira Software (FEI, Bordeaux, France), a 3D visualization program, the cortical area was determined from each sample. Glomerular density was defined as mature glomeruli/cortical area. To determine duration of the nephrogenic zone, kidney sections were stained with *Lotus* lectin to identify the presence of a nephrogenic zone. Cessation of the nephrogenic zone was defined by a lack of cap mesenchyme and the presence of *Lotus* lectin-stained cells just under the capsule.

Study approval. The study was performed according to the Declaration of Helsinki and approved by the National Ethical Review Board. Informed consent was obtained from all participants.

Statistics. For analyses of urine content in patients, one-way ANOVA was used when the populations were normally distributed evaluated by a D'Agostino and Pearson normality test and had variance homogeneity. The number of patients in the DB/FOAR group was too small to analyze for normal distribution. If the groups were not normally distributed or did not have a positive test for variance homogeneity, a nonparametric Kruskal-Wallis test with a Dunn's test for multiple comparisons was performed. When two groups were compared, a Student's *t* test was performed in case of normal distribution and a Mann-Whitney *U* test was performed otherwise.

RESULTS

Renal injury and decline of renal function in murine megalin deficiency. We investigated the role of megalin on renal function in a mouse model of DB/FOAR syndrome. The model is obtained by embryonic kidney-specific KO of megalin (megalin KO) (36, 46). In adult mice, we found reduced kidney function evidenced by decreased GFR [means ± SE, KO mice: 287 ± 25 µL/min vs. wild type (WT) mice: 368 ± 26 µL/min, $P = 0.04$] and slightly increased plasma creatinine (means ± SE; KO mice: 14.4 ± 1.2 µmol/L vs. WT mice: 11.2 ± 0.8 µmol/l; $P = 0.04$) (Fig. 1, *A* and *B*). At this young age, the renal parenchyma from some megalin KO mice revealed areas lacking proximal tubules

Patient	Symbol in figures	Gender	Age	Ethnicity	Pathogenic variant (homozygous)	UA/Crea. mg/mmol (ref: <3 mg/mmol)	UP/Crea. mg/mmol (ref: <15 mg/mmol)	Renal remarks
1-1	★	F	8 Y	UAE	c.7564T>C p.(Y2522H)	NA	260	Hematuria
1-2	★	F	4 Y	UAE	c.7564T>C p.(Y2522H)	NA	203	
2	□	M	35 Y	Portugal	c.857G>T p.(C286F)	10	166	CKD, azotemia, eGFR 17 ml/min/1.73m^2, 1.2-4.7 g protein/24h, occasionally hematuria, atrophic kidneys
3	■	F	12 Y	Belgium	c.7564T>C p.(Y2522H) & c.12623C>A p.(P4208H)	33	225	Normal renal morphology
4-1	✘	F	21 Y	Sweden	c.2639+1G>A (splicesite)	7	124	FSGS, eGFR <60 ml/min/1.73m^2
4-2	○	F	27 Y	Sweden	c.2639+1G>A (splicesite)	12	126	FSGS, eGFR <40 ml/min/1.73m^2
5	●	M	3 M	India	c.13139_13140insC	76	704	
6-1	▲	M	11 Y	Italy	c.9575G>A p.(R3192Q)	21	222	CKD, eGFR 68 ml/min/1.73m^2, mild phosphate leak, hypercalciuria
6-2	◆	F	14 Y	Italy	c.9575G>A p.(R3192Q)	16	221	eGFR 91 ml/min/1.73m^2, mild phosphate leak, hypercalciuria
Carrier	**Symbol in figures**	**Gender**	**Age**	**Ethnicity**	**Pathogenic variant (heterozygous)**	**UA/Crea. mg/mol**	**UP/Crea. mg/mmol**	**Renal remarks**
1a	★	M		UAE	c.7564T>C p.(Y2522H)	NA	28	
2a	■	M	62 Y	Portugal	c.857G>T p.(C286F)	9	46	Simple cyst left kidney
2b	□	F	56 Y	Portugal	c.857G>T p.(C286F)	9	15	Smaller pyelonephritic right kidney
2c	○	F	35 Y	Portugal	c.857G>T p.(C286F)	0.7	13	
2d	▲	F	33 Y	Portugal	c.857G>T p.(C286F)	5	19	
2e	●	F	21 Y	Portugal	c.857G>T p.(C286F)	4	17	
3a	✘	M	-	Belgium	NA	0.5	3	
4a	◆	M	-	Sweden	c.2639+1G>A (splicesite)	0.5	3	
4b	▼	F	-	Sweden	c.2639+1G>A (splicesite)	0.5	3	

Fig. 2. Biochemical and genotype data of Donnai-Barrow/Facio-Oculo-Acoustico-Renal patients and heterozygous carriers. CKD, chronic kidney disease; Crea, creatine; eGFR, estimated glomerular filtration rate; F and M, female and male, respectively; FSGS, focal segmental glomerulosclerosis; UA, urine albumin; UAE, United Arab Emirates; UP, urine protein.

(Fig. 1*C*). In megalin KO mice, we have previously reported urinary excretion of kidney injury markers such as cystatin C (30). As these are megalin ligands, we also investigated injury markers in the urine that are not megalin ligands, which were also elevated in megalin KO mice compared with WT mice, including NAGase (means ± SE, KO mice: 0.08 ± 0.013 U/μmol creatinine vs. WT mice: 0.005 ± 0.0002 U/μmol creatinine, $P < 0.001$) and KIM-1 (means ± SE, KO mice: $10.8 \times 10^6 \pm 1.2 \times 10^6$ arbitrary units/creatinine vs. WT mice: $1.5 \times 10^6 \pm 0.3 \times 10^6$ arbitrary units/creatinine, $P < 0.016$) (Fig. 1, *D* and *E*). These data suggest that megalin deficiency results in renal injury.

DB/FOAR patients demonstrate renal decline. To investigate renal status in the human counterpart of our mouse model, we examined six families with pathogenic variants in the megalin-encoding gene, *LRP2*. Four of the six families were newly identified (*families 1*, *2*, *5*, and *6*; Fig. 2). All patients were homozygous for the pathogenic variant, as shown in Figs. 2 and 3*A*, whereas carriers were heterozygous for the variant. Clinical data from the patients showed urine protein-creatinine levels in the range from 166 to 704 mg/mmol (normal: <15 mg/mmol) and albumin-creatinine levels ranging from 7 to 33 mg/mmol (normal: <3 mg/mmol), indicating a glomerular leak, and four patients had low GFR (Fig. 2). Analyses of patient urine showed

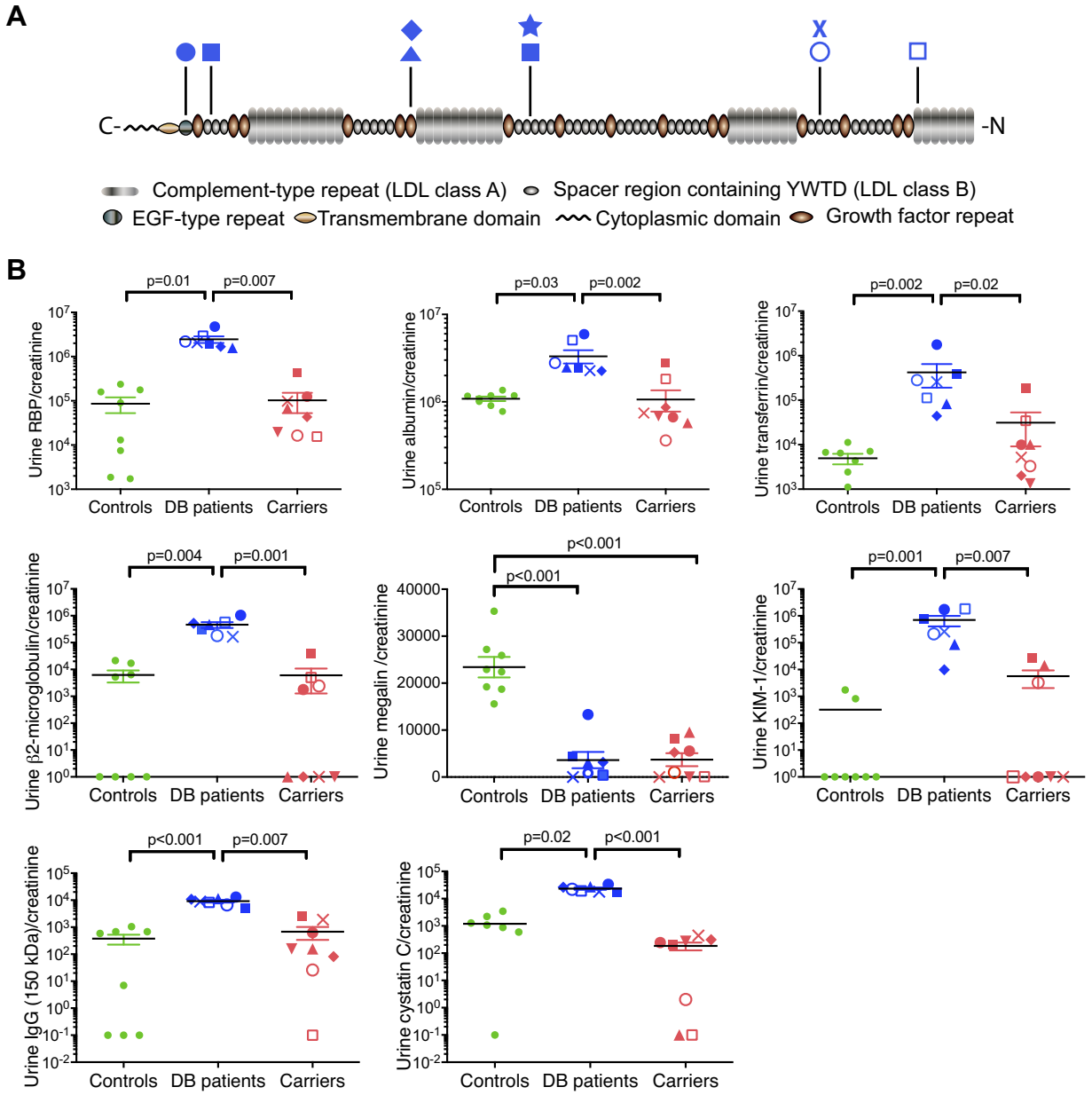

Fig. 3. Localization of pathogenic variants in megalin and urinary profile of Donnai-Barrow/Facio-Oculo-Acoustico-Renal (DB/FOAR) patients and carriers compared with controls. *A*: graphic depiction of megalin with domain organization and identified pathogenic variants. *B*: urinary profile of the following proteins: retinol binding protein (RBP), albumin, transferrin, β_2-microglobulin, megalin, kidney injury molecule-1 (KIM-1), IgG, and cystatin *C*: values for each individual are shown by the symbols from Fig. 2, and the horizontal line indicates means ± SE. The number of data points equals *n*. EGF, epidermal growth factor; LDL, low-density lipoprotein.

elevated excretion of classical megalin and cubilin ligands such as RBP (megalin ligand), transferrin (cubilin ligand), albumin (shared ligand), cystatin C (megalin ligand), and β_2-microglobulin (megalin ligand) compared with controls and carriers (Fig. 3*B* and Supplemental Fig. S2). In addition to low-molecular-weight ligands, we also detected significantly increased excretion of intact (150 kDa) IgG in all patient urines, indicating an effect on the glomerular filtration barrier (Fig. 3*B*). Thus, in addition to low-molecular-weight proteinuria, patients also demonstrated proteinuria of glomerular origin. Furthermore, there was an elevated presence of KIM-1 in all DB/FOAR patients and in three of the carriers from *family 2* (Fig. 3*B*), suggesting renal injury and glomerular dysfunction.

All patients showed a characteristic urinary protein profile that was different from carriers and controls (Supplemental Fig. S3). As expected, DB/FOAR patients from *families 2*, *3*, *4*, and *6* had almost no full-length megalin excretion in the urine, consistent with the absence of megalin protein products. Surprisingly, urinary full-length megalin was also virtually absent in urine from the carriers (Fig. 3*B*).

Analyses of biopsy material (available from *families 1*, *4*, and *6*) showed no brush border immunoreactivity for megalin in *families 4* (41) or *6* (Fig. 4*A*), which has also previously been shown in *family 3* (15). Surprisingly, the two index patients from *family 1* had reduced, normally localized megalin (Fig. 4*A*). Consistent with the remnant presence of the receptor in patients from *family 1*, we detected uptake of ligands like RBP

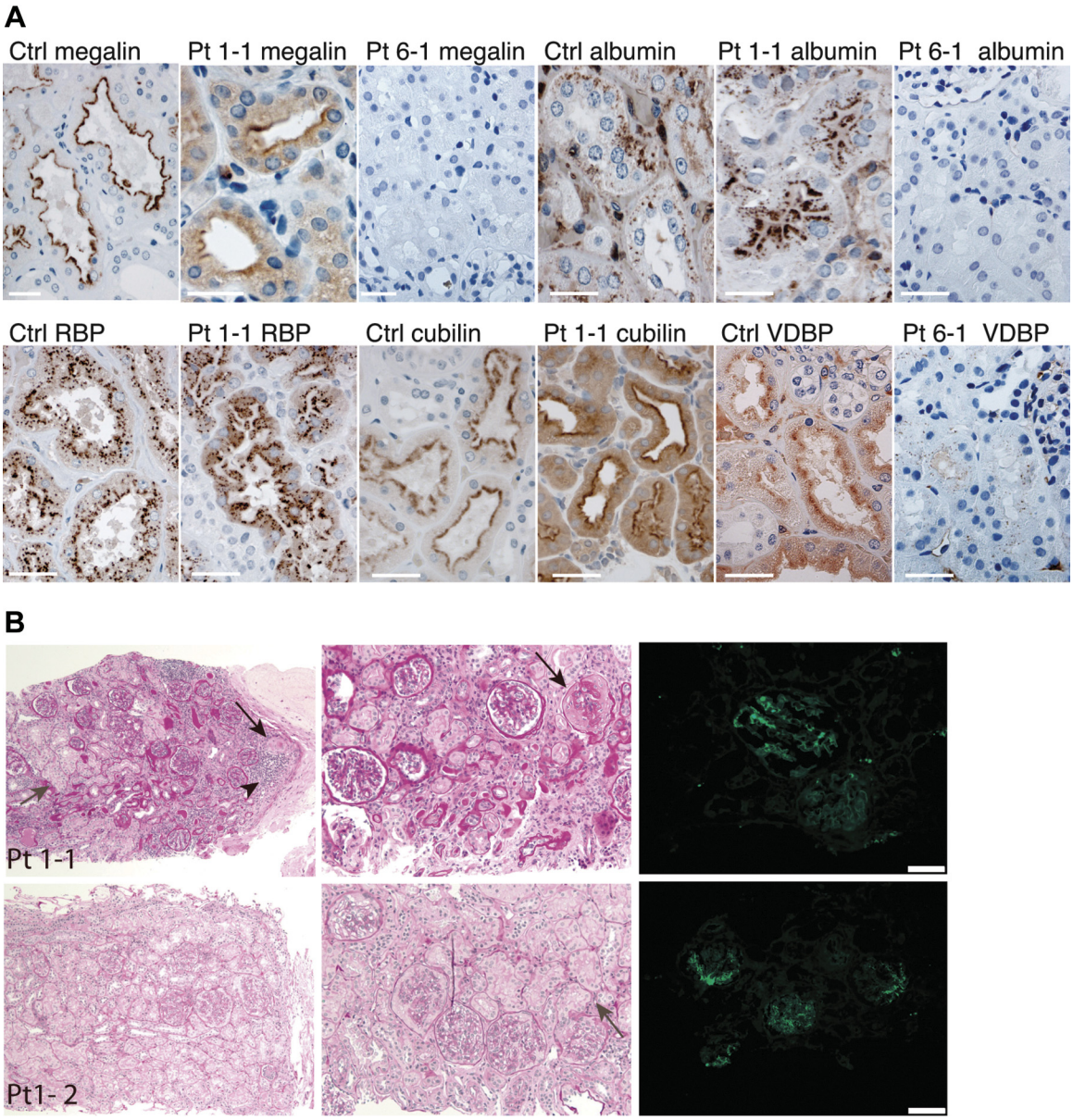

Fig. 4. Proximal tubule endocytic function and renal morphology in Donnai-Barrow/Facio-Oculo-Acoustico-Renal (DB/FOAR) patients and controls (Ctrl). *A*: immunohistochemical staining for proximal tubule receptors and ligands in DB/FOAR patients and controls. Scale bars = 50 μm. *B*: periodic acid-Schiff staining and immunofluorescence analysis of IgA of biopsy material from *patients 1-1* and *1-2*. *Patient 1-1* displays inflammation (arrowhead), hypertrophic tubules (grey arrow), tubular atrophy, and sclerotic glomeruli (black arrow). *Patient 1-2* displays a more well-preserved parenchyma. Scale bars = 200 μm.

and albumin (Fig. 4*A*), which was not present in *families 4* (41) or *6* (Fig. 4*A*). Despite the presence of immunodetectable ligands in patients from *family 1*, they also presented with proteinuria (Fig. 2; unfortunately, urine was inaccessible for further analyses). The presence of proteinuria could be caused by a combination of suboptimal reabsorption (compatible with reduced megalin) and increased glomerular protein leakage. Periodic acid-Schiff staining of kidney biopsy material from *patient 1-1* revealed chronic changes, including focal glomerulosclerosis, interstitial fibrosis, inflammation, and tubular atrophy (Fig. 4*B*). In contrast, *patient 1-2* had fairly well-preserved renal parenchyma (Fig. 4*B*), but the glomeruli from both patients of *family 1* showed signs of advanced renal disease. Some glomeruli were sclerotic, whereas others appeared normal (Fig. 4*B*). Immunofluorescence revealed IgA deposits in all glomeruli investigated in *patient 1-2* and a more focal pattern in *patient 1-1* (Fig. 4*B*). In summary, megalin dysfunction in DB/FOAR patients is associated with proteinuric CKD with glomerular and tubulointerstitial histological lesions.

Nephrogenesis is normal in the megalin-deficient kidney. Megalin is present early in nephrogenesis, which makes it possible that the fully functioning receptor is needed for proper regulation of kidney development through binding and clearing of regulating proteins, such as sonic hedgehog (28, 29). To investigate the mechanism underlying renal decline, we investigated central parameters in nephrogenesis. We examined a cohort of neonatal mice ($n = 3$ mice/group from *postnatal days 0–4*)_ and found that cessation of the nephrogenic zone occurred on *postnatal day 4* in both megalin KO and WT groups, as evidenced by a lack of cap mesenchyme and the presence of *Lotus* lectin-stained cells just under the capsule (Fig. 5*A*). Furthermore, we found that there was no difference in glomerular density at *postnatal day 4* between KO and WT mice (means ± SE, KO mice: $1.3 \pm 0.1/\mu m^2 \times 10^3$ vs. WT mice: $1.2 \pm 0.27/\mu m^2 \times 10^3$, $P = 0.40$; Fig. 5*B*), indicating apparent normal nephrogenesis in megalin KO mice.

Nephron loss and disruption of the glomerulotubular junction in megalin deficiency. To assess whether renal injury resulted in nephron loss in adulthood, we applied CFE-MRI (4, 6–8) to determine the number (N_{glom}) and size (aV_{glom}) of the glomeruli in the adult kidney. We found the megalin KO group had significantly fewer glomeruli than the WT group (means ± SE, KO mice: 9,702 ± 219 vs. WT mice: 12,056 ± 42, $P < 0.001$; Fig. 6*A*) at 50–70 days. At 1 yr of age, the deposition of cationic ferritin in glomeruli of KO mice was virtually absent, whereas in WT mice, the deposition appeared normal (Supplemental Fig. S1), indicating a change of charge or size selectivity of the filtration barrier of megalin-deficient mice. No difference in glomerular volume was observed by MRI (aV_{glom}) between the megalin KO and WT groups (means ± SE, KO mice: $3.3 \pm 0.1\ mm^3 \times 10^{-4}$ vs. WT mice: $3.1 \pm 0.2\ mm^3 \times 10^{-4}$, $P = 0.62$; Fig. 6*B*), and the intrarenal distribution of the volume of glomeruli was unchanged (Fig. 6*C*), indicating there was not a population of small and large glomeruli in either group. The proximal tubule fraction was lower in the megalin KO group compared with the WT group measured as the area of *Lotus*-positive cells in the subcapsular region (means ± SE, KO mice: 42 ± 1.2% vs. WT mice: 46 ± 1.4%, $P = 0.03$; Fig. 6*D*). This was supported by MRI analyses showing a

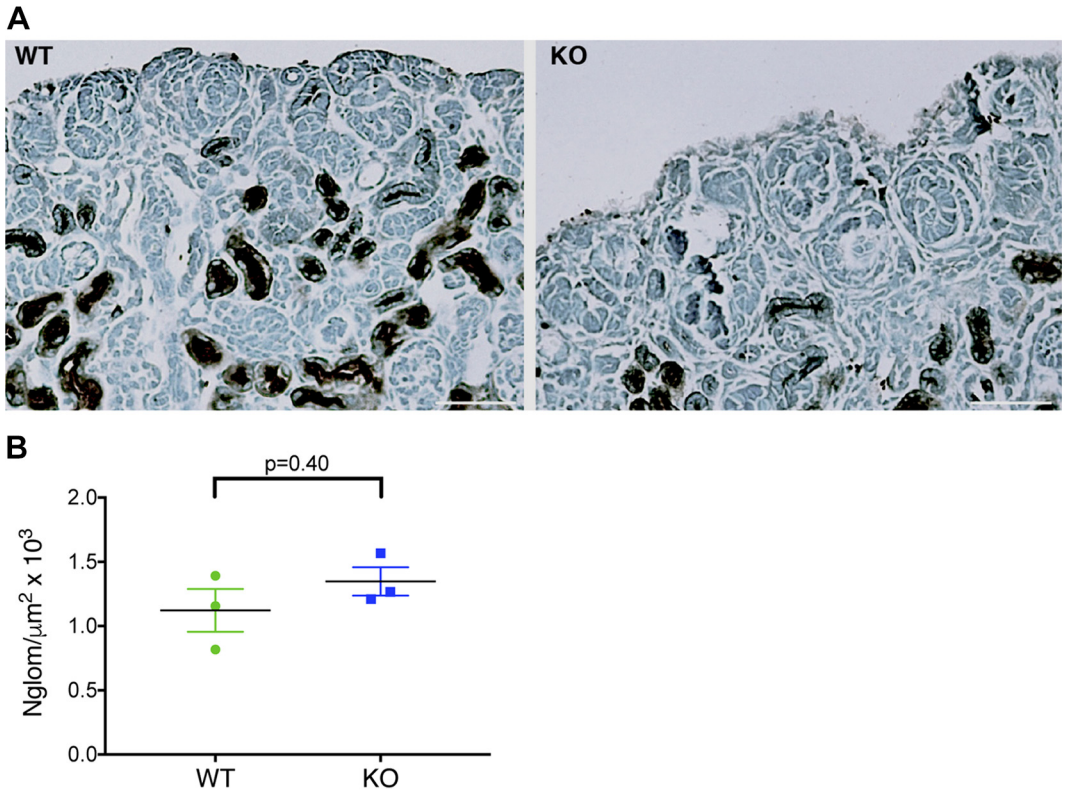

Fig. 5. Nephrogenesis in megalin knockout (KO) and wild-type (WT) mice at *postnatal day 4*. *A*: micrographs of kidney sections from megalin KO and WT-stained with *Lotus tetragonolobus* lectin to identify the presence of the nephrogenic zone. Scale bars = 200 μm. *B*: glomerular density at *postnatal day 4*. N_{glom}, number of glomeruli.

smaller kidney volume in the megalin KO group (means ± SE, KO mice: $1.1 \times 10^{11} \pm 5.5 \times 10^{9}$ µm³ vs. WT mice: $1.3 \times 10^{11} \pm 4.7 \times 10^{9}$ µm³, $P = 0.006$; Fig. 6*E*) and smaller cortical volume in the megalin KO group (means ± SE, KO mice: $6.2 \times 10^{10} \pm 3.1 \times 10^{9}$ µm³ vs. WT mice: $7.7 \times 10^{10} \pm 2.7 \times 10^{9}$ µm³, $P = 0.002$; Fig. 6*F*), but no change in medullary volume between the groups (means ± SE; KO mice: $4.8 \times 10^{10} \pm 3.1 \times 10^{9}$ µm³ vs. WT mice: $4.9 \times 10^{10} \pm 2.9 \times 10^{9}$ µm³, $P = 0.8$; Fig. 6*G*). In the 50- to 70-day group, the health of the glomerulotubular junction was compromised; the fraction of *Lotus*-negative glomeruli (true atubular glomeruli + glomeruli cut at a plane not assessing the junction) was greater in the KO group than in the WT group (means ± SE, KO mice: 32 ± 2.6% vs. WT mice: 25 ± 1.5%, $P = 0.048$; Fig. 6*H*). Our findings demonstrate that in WT mice, *Lotus* lectin is not detectable in Bowman's capsule in ~25% of the glomeruli, secondary to the direction of the sectioned tissue. However, in megalin KO mice, the percentage of *Lotus*-negative glomeruli was 7% higher than in WT mice, reflecting a population of atubular glomeruli. Thus, at 8–10 wk of age megalin KO mice have lost ~19% of their glomeruli and another 7% have an

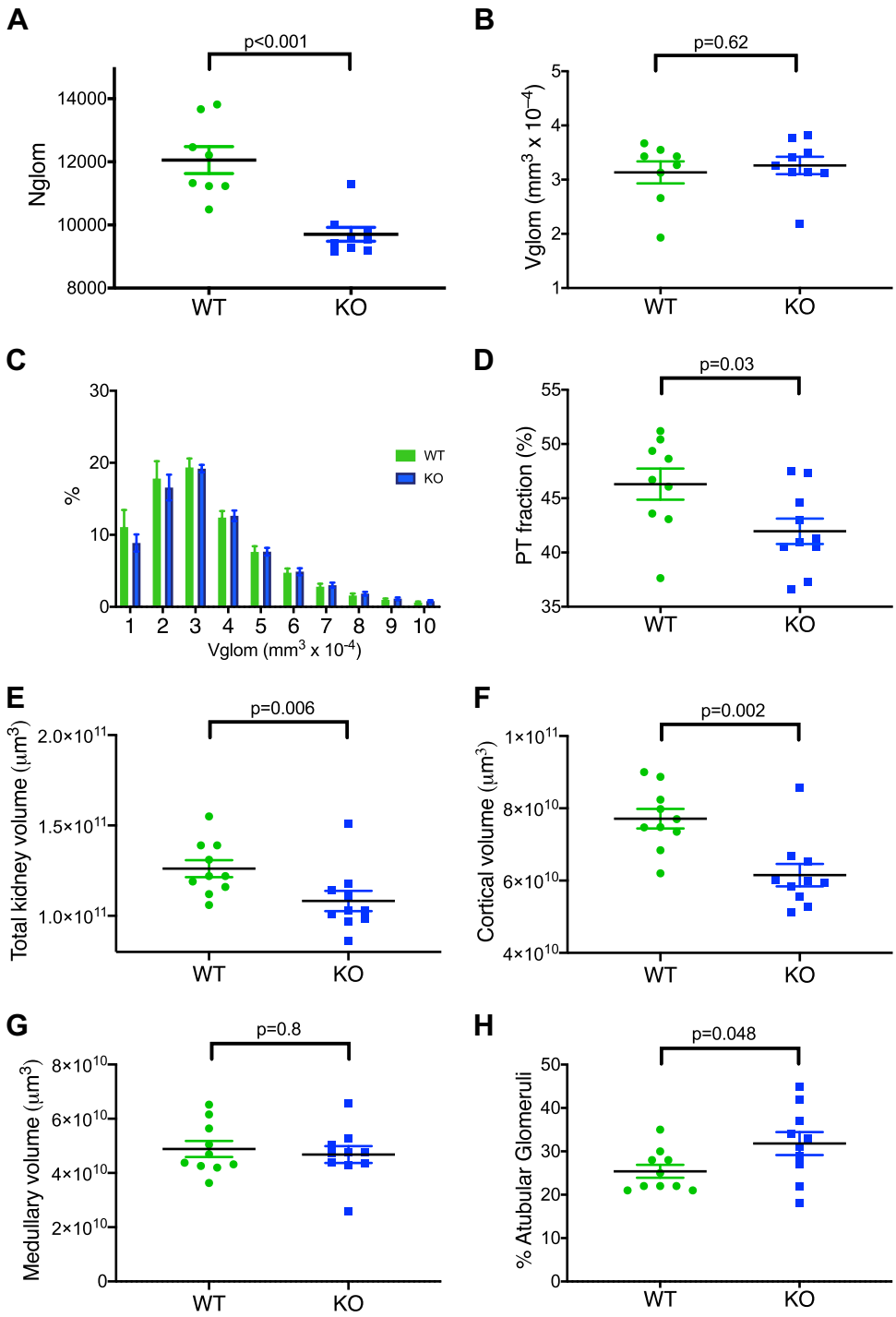

Fig. 6. Analyses of renal structure in megalin knockout (KO) and wild-type (WT) mice at 50–70 days. *A*: number of glomeruli (N_{glom}). *B*: volume of glomeruli (V_{glom}). *C*: distribution as a percentage of glomerular volume. *D*: proximal tubule (PT) fraction as a percentage. *E*: total kidney volume. *F*: cortical volume. *G*: medullary volume. *H*: fraction of atubular glomeruli. In *C*, $n = 5$ animals in each group encompassing 9–12,000 glomeruli. In all other graphs, n = the number of data points. Values for each individual mouse are shown by a symbol, and the horizontal line indicates means ± SE.

abnormal glomerulotubular junction, which will likely result in their loss with time. Taken together, these analyses suggest that glomerulotubular disconnection and nephron loss are a result of megalin dysfunction.

DISCUSSION

In this study, we aimed to establish whether megalin deficiency or dysfunction plays a role in progressive kidney disease. We found that renal function was affected by megalin dysfunction in both our mouse model and human subjects (Fig. 7). The absence of megalin in mice resulted in renal decline, disruption of the glomerulotubular junction, and nephron loss early in adulthood without an overt effect on nephrogenesis. To validate the renal decline observed in our mouse model in humans, we included six families with pathogenic variants in *LRP2*, to investigate the impact of these variants on renal health. All patients presented with tubular dysfunction, which was apparent by the urinary loss of megalin-cubilin ligands, consistent with megalin dysfunction. In addition, patients experienced urinary loss of high-molecular-weight proteins like immunoglobulins and transferrin indicative of an affected glomerular filtration barrier. Supportive of a glomerular component of the proteinuria, patients had urinary protein and albumin excretion, which was higher than that of low-molecular-weight proteinuria. Furthermore, several patients had a low GFR (23) and a clinical diagnosis of CKD. In addition, all patients had elevated levels of urinary KIM-1. Urinary KIM-1 has been correlated with inflammation and proximal tubule injury and has been shown to be a biomarker of renal injury and risk of CKD (37). Altogether, our data strongly suggest that megalin dysfunction poses an increased risk of renal decline, involving both the tubules and glomeruli. Our study is in line with a genome-wide association study showing that single nucleotide polymorphisms in *LRP2* are associated with low GFR (10), and we speculate that milder forms of the disease might contribute to the population of patients with CKD without known etiology. As megalin is present both in podocytes and tubules, future work will focus on the role of megalin in the glomeruli along with ligand loss as potential contributors to kidney decline and their role in CKD progression.

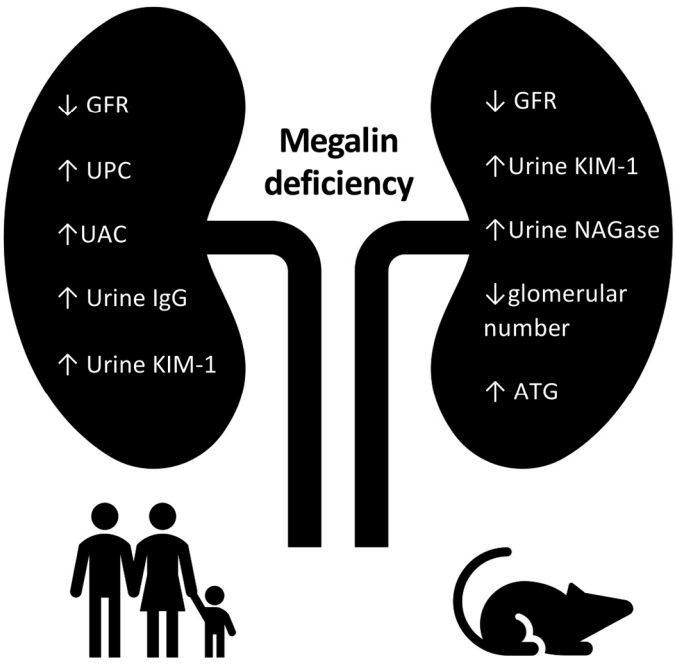

Fig. 7. Schematic summary of the renal findings early in the life of Donnai-Barrow/Facio-Oculo-Acoustico-Renal (DB/FOAR) patients and mice. In patients, low glomerular filtration rate (GFR) was detected, whereas urinary excretion of protein (UPC, urine protein-to-creatinine ratio), albumin (UAC, urine albumin-to-creatinine ratio), high-molecular-weight proteins (Ig), and kidney injury molecule-1(KIM-1) were elevated. In megalin knockout mice, we also found lower GFR, elevated urinary excretion of KIM-1 and *N*-acetyl-β-D-glucosaminidase (NAGase), fewer glomeruli, and increased number of atubular glomeruli (ATG).

Currently, the role of megalin in podocytes has not been entirely clarified. Megalin appears to have endocytic function. It was originally described as the Heyman nephritis antigen in rats (21, 22, 31), but it has not been demonstrated to be involved in human nephritis. In *family 1*, immunofluorescence revealed IgA deposits; in *patient 1-1*, all investigated glomeruli were affected, whereas in *patient 1-2*, a more focal pattern was present. We speculate that the remnant immunoreactive megalin product may be antigenic in this family. Besides this glomerular change in this family, our patient data demonstrated that the filtration barrier was affected, indicating a role of megalin in podocyte health. Significant glomerular changes were also present in our mouse model, where at 1 yr of age, the deposition of cationic ferritin in KO was almost absent compared with controls. As CFE deposition requires a negatively charged filtration barrier and a barrier that retains it, this indicates that the filtration barrier is changed either with regard to charge or size selectivity, which points at a role of megalin in the maintenance of podocyte function. Thus, the lack of megalin in podocytes could potentially contribute to renal decline and loss of the glomerulotubular junction.

To clarify the underlying mechanism of kidney disease, as we know that megalin is present throughout nephrogenesis (3, 33), we used a mouse model with embryonic kidney-specific megalin KO to investigate whether the absence of the receptor influences nephron formation (46). We did not find any significant changes in nephrogenesis or early postnatal glomerular density but a significant impact on renal structure, renal function, and nephron abundance in early adulthood. Thus, our data suggest that nephron survival postnatally is affected in the megalin-deficient state, which is in line with an earlier report of increased apoptotic cell numbers in megalin-negative cells observed by Theilig et al. (43) in a mosaic megalin KO model. Further work is needed to differentiate the direct effect of the loss of megalin ligands in the urine versus the lack of the megalin receptor per se. Deficiency of megalin ligands, including the lack of uptake of antiapoptotic proteins such as survivin (19), may play a role in maintenance of the glomerulotubular connection and nephron survival. Recently, it has been shown that albumin loss as the consequence of cubilin variants does not cause kidney disease (5), indicating that the loss of albumin and potentially other cubilin ligands (which are much fewer that megalin ligands) does not affect renal health in humans (30). Thus, further work is necessary to determine whether replacement of some specific megalin ligands could improve overall renal health or whether other yet unknown functions of megalin in both podocytes and the tubules could play a role.

The presence (although in low levels) of immunoreactive megalin and ligands in the proximal tubules of *patients 1-1* and

1-2 was rather unexpected. The existence of DB/FOAR patients with megalin expression has also been reported by Kantarci et al. (20), supporting that DB/FOAR syndrome can develop despite the presence of an immunoreactive protein product. The pathogenic variant in *family 1* interferes with the YWTD repeat in a LDL class B domain changing Y into H. In the LDL receptor, these repeats are involved in pH-dependent release of ligands in the endosomal compartment (16). Therefore, it is possible that the variant results in a protein product but restricts ligand dissociation leading to *1*) recycling of the whole ligand-receptor complex and *2*) a disturbed endocytic process. Recently, Flemming et al. (17) demonstrated that the pathogenic variant present in *family 6* interferes with receptor-ligand dissociation and causes aberrant trafficking of megalin for lysosomal degradation. A similar mechanism could play a role in the reduced megalin abundance that we observed in *family 1*. We cannot exclude that the remnant receptor expression in *family 1* mediates endocytosis, but that this is insufficient to avoid protein leakage into the urine combined with the presence of an affected filtration barrier leading to increased filtration.

In conclusion, our study shows pathogenic variants in *LRP2* as an etiology for early onset of CKD, which could also include patients without the advanced DB/FOAR phenotype pointing to awareness of this as a cause of CKD without a clear etiology. We document that megalin dysfunction is associated with proximal tubular and glomerular dysfunction and disruption of the glomerulotubular junction with subsequent nephron loss, which most likely contributes to the development or progression of CKD.

ACKNOWLEDGMENTS

We are grateful for the excellent technical assistance of Hanne Sidelmann, Pia K. Nielsen, Helle Gittens, Inger Kristoffersen, and Kimberly deRonde. We also thank the Yale Center for Mendelian Genomics for whole exome sequencing analysis (U54HG006504).

A.C. was on leave from the University of Warsaw, Warsaw, Poland.

GRANTS

This work was supported by the Danish Medical Research Council, Augustinus Foundation, Edith Waagens og Frode Waagens Foundation, Novo Nordisk Foundation, Jens Ove Jakobsen Foundation, and Bruker ClinScan 7T MRI in the Molecular Imaging Core, which was purchased with support from National Institutes of Health (NIH) Grant 1S10RR01991101 and is supported by the University of Virginia School of Medicine. J.R.C. and K.M.B. received funding from NIH Grants R01DK110622 and R01DK111861. F.H. received funding from NIH Grant DK0668306. F.J. is a Fellow of the Fonds National de la Recherche Scientifique in Belgium.

DISCLOSURES

No conflicts of interest, financial or otherwise, are declared by the authors.

AUTHOR CONTRIBUTIONS

J.R.C., R.N., W.T. and S.R. conceived and designed research; J.R.C., F.J., J.O., C.F., S.M., F.H., T.S., T.S., E.C., R.N., W.T., G.D., L.T., S.R., A.C., S.N. and F.E. performed experiments; J.R.C., J.O., L.T., C.F., S.M., F.H., T.S., T.S., E.C., R.N., W.T., G.D., L.T., S.R., K.M.B. and A.C. analyzed data; J.R.C., F.J., J.O., E.C., R.N., W.T., G.D., L.T., S.R., K.M.B. and F.E. interpreted results of experiments; J.R.C., R.N. and A.C. prepared figures; J.R.C., R.N. and W.T. drafted manuscript; J.R.C., F.J., J.O., L.T., C.F., T.S., T.S., E.C., R.N., W.T., S.R., K.M.B., A.C., S.N. and F.E. edited and revised manuscript; J.R.C., F.J., J.O., L.T., C.F., S.M., F.H., T.S., T.S., E.C., R.N., W.T., G.D., L.T., S.R., K.M.B., A.C., S.N. and F.E. approved final version of manuscript.

REFERENCES

1. **Amsellem S, Gburek J, Hamard G, Nielsen R, Willnow TE, Devuyst O, Nexo E, Verroust PJ, Christensen EI, Kozyraki R.** Cubilin is essential for albumin reabsorption in the renal proximal tubule. *J Am Soc Nephrol* 21: 1859–1867, 2010. doi:10.1681/ASN.2010050492.
2. **Anglani F, Terrin L, Brugnara M, Battista M, Cantaluppi V, Ceol M, Bertoldi L, Valle G, Joy MP, Pober BR, Longoni M.** Hypercalciuria and nephrolithiasis: expanding the renal phenotype of Donnai-Barrow syndrome. *Clin Genet* 94: 187–188, 2018. doi:10.1111/cge.13242.
3. **Assémat E, Châtelet F, Chandellier J, Commo F, Cases O, Verroust P, Kozyraki R.** Overlapping expression patterns of the multiligand endocytic receptors cubilin and megalin in the CNS, sensory organs and developing epithelia of the rodent embryo. *Gene Expr Patterns* 6: 69–78, 2005. doi:10.1016/j.modgep.2005.04.014.
4. **Baldelomar EJ, Charlton JR, Beeman SC, Hann BD, Cullen-McEwen L, Pearl VM, Bertram JF, Wu T, Zhang M, Bennett KM.** Phenotyping by magnetic resonance imaging nondestructively measures glomerular number and volume distribution in mice with and without nephron reduction. *Kidney Int* 89: 498–505, 2016. doi:10.1038/ki.2015.316.
5. **Bedin M, Boyer O, Servais A, Li Y, Villoing-Gaude L, Tete MJ, Cambier A, Hogan J, Baudouin V, Krid S, Bensman A, Lammens F, Louillet F, Ranchin B, Vigneau C, Bouteau I, Isnard-Bagnis C, Mache CJ, Schafer T, Pape L, Godel M, Huber TB, Benz M, Klaus G, Hansen M, Latta K, Gribouval O, Moriniere V, Tournant C, Grohmann M, Kuhn E, Wagner T, Bole-Feysot C, Jabot-Hanin F, Nitschke P, Ahluwalia TS, Kottgen A, Andersen CBF, Bergmann C, Antignac C, Simons M.** Human C-terminal CUBN variants associate with chronic proteinuria and normal renal function. *J Clin Invest* 130: 335–344, 2019. doi:10.1172/JCI129937.
6. **Beeman SC, Cullen-McEwen LA, Puelles VG, Zhang M, Wu T, Baldelomar EJ, Dowling J, Charlton JR, Forbes MS, Ng A, Wu QZ, Armitage JA, Egan GF, Bertram JF, Bennett KM.** MRI-based glomerular morphology and pathology in whole human kidneys. *Am J Physiol Renal Physiol* 306: F1381–F1390, 2014. doi:10.1152/ajprenal.00092.2014.
7. **Beeman SC, Zhang M, Gubhaju L, Wu T, Bertram JF, Frakes DH, Cherry BR, Bennett KM.** Measuring glomerular number and size in perfused kidneys using MRI. *Am J Physiol Renal Physiol* 300: F1454–F1457, 2011. doi:10.1152/ajprenal.00044.2011.
8. **Bennett KM, Zhou H, Sumner JP, Dodd SJ, Bouraoud N, Doi K, Star RA, Koretsky AP.** MRI of the basement membrane using charged nanoparticles as contrast agents. *Magn Reson Med* 60: 564–574, 2008. doi:10.1002/mrm.21684.
9. **Charlton JR, Baldelomar EJ, deRonde KA, Cathro HP, Charlton NP, Criswell SJ, Hyatt DM, Nam S, Pearl V, Bennett KM.** Nephron loss detected by MRI following neonatal acute kidney injury in rabbits. *Pediatr Res* 87: 1185−1192, 2020. doi:10.1038/s41390-019-0684-1.
10. **Chasman DI, Fuchsberger C, Pattaro C, Teumer A, Böger CA, Endlich K, Olden M, Chen MH, Tin A, Taliun D, Li M, Gao X, Gorski M, Yang Q, Hundertmark C, Foster MC, O'Seaghdha CM, Glazer N, Isaacs A, Liu CT, Smith AV, O'Connell JR, Struchalin M, Tanaka T, Li G, Johnson AD, Gierman HJ, Feitosa MF, Hwang SJ, Atkinson EJ, Lohman K, Cornelis MC, Johansson A, Tönjes A, Dehghan A, Lambert JC, Holliday EG, Sorice R, Kutalik Z, Lehtimäki T, Esko T, Deshmukh H, Ulivi S, Chu AY, Murgia F, Trompet S, Imboden M, Coassin S, Pistis G, Harris TB, Launer LJ, Aspelund T, Eiriksdottir G, Mitchell BD, Boerwinkle E, Schmidt H, Cavalieri M, Rao M, Hu F, Demirkan A, Oostra BA, de Andrade M, Turner ST, Ding J, Andrews JS, Freedman BI, Giulianini F, Koenig W, Illig T, Meisinger C, Gieger C, Zgaga L, Zemunik T, Boban M, Minelli C, Wheeler HE, Igl W, Zaboli G, Wild SH, Wright AF, Campbell H, Ellinghaus D, Nöthlings U, Jacobs G, Biffar R, Ernst F, Homuth G, Kroemer HK, Nauck M, Stracke S, Völker U, Völzke H, Kovacs P, Stumvoll M, Mägi R, Hofman A, Uitterlinden AG, Rivadeneira F, Aulchenko YS, Polasek O, Hastie N, Vitart V, Helmer C, Wang JJ, Stengel B, Ruggiero D, Bergmann S, Kähönen M, Viikari J, Nikopensius T, Province M, Ketkar S, Colhoun H, Doney A, Robino A, Krämer BK, Portas L, Ford I, Buckley BM, Adam M, Thun GA, Paulweber B, Haun M, Sala C, Mitchell P, Ciullo M, Kim SK, Vollenweider P, Raitakari O, Metspalu A, Palmer C, Gasparini P, Pirastu M, Jukema JW, Probst-Hensch NM, Kronenberg F, Toniolo D, Gudnason V, Shuldiner AR, Coresh J, Schmidt R,**

Ferrucci L, **Siscovick DS**, **van Duijn CM**, **Borecki IB**, **Kardia SL**, **Liu Y**, **Curhan GC**, **Rudan I**, **Gyllensten U**, **Wilson JF**, **Franke A**, **Pramstaller PP**, **Rettig R**, **Prokopenko I**, **Witteman J**, **Hayward C**, **Ridker PM**, **Parsa A**, **Bochud M**, **Heid IM**, **Kao WH**, **Fox CS**, **Köttgen A**; **CARDIoGRAM Consortium**; **ICBP Consortium**; **CARe Consortium**; **WTCCC2.** Integration of genome-wide association studies with biological knowledge identifies six novel genes related to kidney function. *Hum Mol Genet* 21: 5329–5343, 2012. doi:10.1093/hmg/dds369.

11. **Chatelet F**, **Brianti E**, **Ronco P**, **Roland J**, **Verroust P.** Ultrastructural localization by monoclonal antibodies of brush border antigens expressed by glomeruli. I. Renal distribution. *Am J Pathol* 122: 500–511, 1986.
12. **Christensen EI**, **Birn H**, **Storm T**, **Weyer K**, **Nielsen R.** Endocytic receptors in the renal proximal tubule. *Physiology (Bethesda)* 27: 223–236, 2012. doi:10.1152/physiol.00022.2012.
13. **Christensen EI**, **Gliemann J**, **Moestrup SK.** Renal tubule gp330 is a calcium binding receptor for endocytic uptake of protein. *J Histochem Cytochem* 40: 1481–1490, 1992. doi:10.1177/40.10.1382088.
14. **Christensen EI**, **Nielsen S**, **Moestrup SK**, **Borre C**, **Maunsbach AB**, **de Heer E**, **Ronco P**, **Hammond TG**, **Verroust P.** Segmental distribution of the endocytosis receptor gp330 in renal proximal tubules. *Eur J Cell Biol* 66: 349–364, 1995.
15. **Dachy A**, **Paquot F**, **Debray G**, **Bovy C**, **Christensen EI**, **Collard L**, **Jouret F.** In-depth phenotyping of a Donnai-Barrow patient helps clarify proximal tubule dysfunction. *Pediatr Nephrol* 30: 1027–1031, 2015. doi:10.1007/s00467-014-3037-7.
16. **Davis CG**, **Goldstein JL**, **Südhof TC**, **Anderson RG**, **Russell DW**, **Brown MS.** Acid-dependent ligand dissociation and recycling of LDL receptor mediated by growth factor homology region. *Nature* 326: 760–765, 1987. doi:10.1038/326760a0.
17. **Flemming JM**, **Marczenke M**, **Rudolph I-M**, **Nielsen R**, **Storm T**, **Erik IC**, **Diecke S**, **Emma F**, **Willnow TE.** Induced pluripotent stem cell-based disease modeling identifies ligand-induced decay of megalin as a cause of Donnai-Barrow syndrome. *Kidney Int* 98: 159–167, 2020. doi:10.1016/j.kint.2020.02.021.
18. **Galarreta CI**, **Grantham JJ**, **Forbes MS**, **Maser RL**, **Wallace DP**, **Chevalier RL.** Tubular obstruction leads to progressive proximal tubular injury and atubular glomeruli in polycystic kidney disease. *Am J Pathol* 184: 1957–1966, 2014. doi:10.1016/j.ajpath.2014.03.007.
19. **Jobst-Schwan T**, **Knaup KX**, **Nielsen R**, **Hackenbeck T**, **Buettner-Herold M**, **Lechler P**, **Kroening S**, **Goppelt-Struebe M**, **Schloetzer-Schrehardt U**, **Fürnrohr BG**, **Voll RE**, **Amann K**, **Eckardt KU**, **Christensen EI**, **Wiesener MS.** Renal uptake of the antiapoptotic protein survivin is mediated by megalin at the apical membrane of the proximal tubule. *Am J Physiol Renal Physiol* 305: F734–F744, 2013. doi:10.1152/ajprenal.00546.2012.
20. **Kantarci S**, **Al-Gazali L**, **Hill RS**, **Donnai D**, **Black GC**, **Bieth E**, **Chassaing N**, **Lacombe D**, **Devriendt K**, **Teebi A**, **Loscertales M**, **Robson C**, **Liu T**, **MacLaughlin DT**, **Noonan KM**, **Russell MK**, **Walsh CA**, **Donahoe PK**, **Pober BR.** Mutations in LRP2, which encodes the multiligand receptor megalin, cause Donnai-Barrow and facio-oculo-acoustico-renal syndromes. *Nat Genet* 39: 957–959, 2007. doi:10.1038/ng2063.
21. **Kerjaschki D**, **Farquhar MG.** Immunocytochemical localization of the Heymann nephritis antigen (GP330) in glomerular epithelial cells of normal Lewis rats. *J Exp Med* 157: 667–686, 1983. doi:10.1084/jem.157.2.667.
22. **Kerjaschki D**, **Farquhar MG.** The pathogenic antigen of Heymann nephritis is a membrane glycoprotein of the renal proximal tubule brush border. *Proc Natl Acad Sci USA* 79: 5557–5561, 1982. doi:10.1073/pnas.79.18.5557.
23. **Ketteler M**, **Block GA**, **Evenepoel P**, **Fukagawa M**, **Herzog CA**, **McCann L**, **Moe SM**, **Shroff R**, **Tonelli MA**, **Toussaint ND**, **Vervloet MG**, **Leonard MB.** Diagnosis, evaluation, prevention, and treatment of chronic kidney disease-mineral and bone disorder: synopsis of the Kidney Disease: Improving Global Outcomes 2017 clinical practice guideline update. *Ann Intern Med* 168: 422–430, 2018. doi:10.7326/M17-2640.
24. **Kumar GC**, **Chaudhry M**, **Mohamed Faris KMM**, **Al Masri O.** Renal involvement in a child with Donnai Barrow syndrome. *Asian J Pediatr Nephrol* 1: 93–95, 2018. doi:10.4103/AJPN.AJPN_22_18.
25. **Larsen T**, **Rontved CM**, **Ingvartsen KL**, **Vels L**, **Bjerring M.** Enzyme activity and acute phase proteins in milk utilized as indicators of acute clinical *E. coli* LPS-induced mastitis. *Animal* 4: 1672−1679, 2010. doi:10.1017/S1751731110000947.
26. **Le Panse S**, **Galceran M**, **Pontillon F**, **Lelongt B**, **van de Putte M**, **Ronco PM**, **Verroust PJ.** Immunofunctional properties of a yolk sac epithelial cell line expressing two proteins gp280 and gp330 of the intermicrovillar area of proximal tubule cells: inhibition of endocytosis by the specific antibodies. *Eur J Cell Biol* 67: 120–129, 1995.
27. **Leheste JR**, **Rolinski B**, **Vorum H**, **Hilpert J**, **Nykjaer A**, **Jacobsen C**, **Aucouturier P**, **Moskaug JO**, **Otto A**, **Christensen EI**, **Willnow TE.** Megalin knockout mice as an animal model of low molecular weight proteinuria. *Am J Pathol* 155: 1361–1370, 1999. doi:10.1016/S0002-9440(10)65238-8.
28. **McCarthy RA**, **Barth JL**, **Chintalapudi MR**, **Knaak C**, **Argraves WS.** Megalin functions as an endocytic sonic hedgehog receptor. *J Biol Chem* 277: 25660–25667, 2002. doi:10.1074/jbc.M201933200.
29. **Morales CR**, **Zeng J**, **El Alfy M**, **Barth JL**, **Chintalapudi MR**, **McCarthy RA**, **Incardona JP**, **Argraves WS.** Epithelial trafficking of Sonic hedgehog by megalin. *J Histochem Cytochem* 54: 1115–1127, 2006. doi:10.1369/jhc.5A6899.2006.
30. **Nielsen R**, **Christensen EI**, **Birn H.** Megalin and cubilin in proximal tubule protein reabsorption: from experimental models to human disease. *Kidney Int* 89: 58–67, 2016. doi:10.1016/j.kint.2015.11.007.
31. **Prabakaran T**, **Nielsen R**, **Larsen JV**, **Sørensen SS**, **Feldt-Rasmussen U**, **Saleem MA**, **Petersen CM**, **Verroust PJ**, **Christensen EI.** Receptor-mediated endocytosis of α-galactosidase A in human podocytes in Fabry disease. *PLoS One* 6: e25065–e25076, 2011. doi:10.1371/journal.pone.0025065.
32. **Rieg T.** A High-throughput method for measurement of glomerular filtration rate in conscious mice. *J Vis Exp* 2013: e50330, 2013. doi:10.3791/50330.
33. **Sahali D**, **Mulliez N**, **Chatelet F**, **Laurent-Winter C**, **Citadelle D**, **Sabourin JC**, **Roux C**, **Ronco P**, **Verroust P.** Comparative immunochemistry and ontogeny of two closely related coated pit proteins. The 280-kd target of teratogenic antibodies and the 330-kd target of nephritogenic antibodies. *Am J Pathol* 142: 1654–1667, 1993.
34. **Schrauwen I**, **Sommen M**, **Claes C**, **Pinner J**, **Flaherty M**, **Collins F**, **Van Camp G.** Broadening the phenotype of LRP2 mutations: a new mutation in LRP2 causes a predominantly ocular phenotype suggestive of Stickler syndrome. *Clin Genet* 86: 282–286, 2014. doi:10.1111/cge.12265.
35. **Shaheen IS**, **Finlay E**, **Prescott K**, **Russell M**, **Longoni M**, **Joss S.** Focal segmental glomerulosclerosis in a female patient with Donnai-Barrow syndrome. *Clin Dysmorphol* 19: 35–37, 2010. doi:10.1097/MCD.0b013e328333c20a.
36. **Shan J**, **Jokela T**, **Skovorodkin I**, **Vainio S.** Mapping of the fate of cell lineages generated from cells that express the Wnt4 gene by time-lapse during kidney development. *Differentiation* 79: 57–64, 2010. doi:10.1016/j.diff.2009.08.006.
37. **Song J**, **Yu J**, **Prayogo GW**, **Cao W**, **Wu Y**, **Jia Z**, **Zhang A.** Understanding kidney injury molecule 1: a novel immune factor in kidney pathophysiology. *Am J Transl Res* 11: 1219–1229, 2019.
38. **Stora S**, **Conte M**, **Chouery E**, **Richa S**, **Jalkh N**, **Gillart AC**, **Joannis AL**, **Mégarbané A.** A 56-year-old female patient with facio-oculo-acoustico-renal syndrome (FOAR) syndrome. Report on the natural history and of a novel mutation. *Eur J Med Genet* 52: 341–343, 2009. doi:10.1016/j.ejmg.2009.06.005.
39. **Storm T**, **Christensen EI**, **Christensen JN**, **Kjaergaard T**, **Uldbjerg N**, **Larsen A**, **Honoré B**, **Madsen M.** Megalin is predominantly observed in vesicular structures in first and third trimester cytotrophoblasts of the human placenta. *J Histochem Cytochem* 64: 769–784, 2016. doi:10.1369/0022155416672210.
40. **Storm T**, **Heegaard S**, **Christensen EI**, **Nielsen R.** Megalin-deficiency causes high myopia, retinal pigment epithelium-macromelanosomes and abnormal development of the ciliary body in mice. *Cell Tissue Res* 358: 99–107, 2014. doi:10.1007/s00441-014-1919-4.
41. **Storm T**, **Tranebjærg L**, **Frykholm C**, **Birn H**, **Verroust PJ**, **Nevéus T**, **Sundelin B**, **Hertz JM**, **Holmström G**, **Ericson K**, **Christensen EI**, **Nielsen R.** Renal phenotypic investigations of megalin-deficient patients: novel insights into tubular proteinuria and albumin filtration. *Nephrol Dial Transplant* 28: 585–591, 2013. doi:10.1093/ndt/gfs462.
42. **Tauris J**, **Christensen EI**, **Nykjaer A**, **Jacobsen C**, **Petersen CM**, **Ovesen T.** Cubilin and megalin co-localize in the neonatal inner ear. *Audiol Neurotol* 14: 267–278, 2009. doi:10.1159/000199446.
43. **Theilig F**, **Kriz W**, **Jerichow T**, **Schrade P**, **Hähnel B**, **Willnow T**, **Le Hir M**, **Bachmann S.** Abrogation of protein uptake through megalin-deficient proximal tubules does not safeguard against tubulointerstitial injury. *J Am Soc Nephrol* 18: 1824–1834, 2007. doi:10.1681/ASN.2006111266.

44. **Vasli N**, **Ahmed I**, **Mittal K**, **Ohadi M**, **Mikhailov A**, **Rafiq MA**, **Bhatti A**, **Carter MT**, **Andrade DM**, **Ayub M**, **Vincent JB**, **John P.** Identification of a homozygous missense mutation in LRP2 and a hemizygous missense mutation in TSPYL2 in a family with mild intellectual disability. *Psychiatr Genet* 26: 66–73, 2016. doi:10.1097/YPG.0000000000000114.
45. **Vinge L**, **Lees GE**, **Nielsen R**, **Kashtan CE**, **Bahr A**, **Christensen EI.** The effect of progressive glomerular disease on megalin-mediated endocytosis in the kidney. *Nephrol Dial Transplant* 25: 2458–2467, 2010. doi:10.1093/ndt/gfq044.
46. **Weyer K**, **Storm T**, **Shan J**, **Vainio S**, **Kozyraki R**, **Verroust PJ**, **Christensen EI**, **Nielsen R.** Mouse model of proximal tubule endocytic dysfunction. *Nephrol Dial Transplant* 26: 3446–3451, 2011. doi:10.1093/ndt/gfr525.
47. **Willnow TE**, **Hilpert J**, **Armstrong SA**, **Rohlmann A**, **Hammer RE**, **Burns DK**, **Herz J.** Defective forebrain development in mice lacking gp330/megalin. *Proc Natl Acad Sci USA* 93: 8460–8464, 1996. doi:10.1073/pnas.93.16.8460.
48. **Yamazaki H**, **Saito A**, **Ooi H**, **Kobayashi N**, **Mundel P**, **Gejyo F.** Differentiation-induced cultured podocytes express endocytically active megalin, a heymann nephritis antigen. *Nephron, Exp Nephrol* 96: e52–e58, 2004. doi:10.1159/000076404.
49. **Zheng G**, **Bachinsky DR**, **Stamenkovic I**, **Strickland DK**, **Brown D**, **Andres G**, **McCluskey RT.** Organ distribution in rats of two members of the low-density lipoprotein receptor gene family, gp330 and LRP/alpha 2MR, and the receptor-associated protein (RAP). *J Histochem Cytochem* 42: 531–542, 1994. doi:10.1177/42.4.7510321.